SCIENCE CHINA
Information Sciences

• Supplementary File •

Identifying the asymmetric superposition of fractional orbital-angular-momentum modes via neural networks with a small dataset

Rong Ma[1], Lihong Li[1], Xiaoqin Qu[1], Jiajie Ning[1],
Jianan Liang[1], Meihong Wang[2,3] & Xiaolong Su[2,3*]

[1]*College of Physics and Electronic Engineering, Shanxi University, Taiyuan* 030006*, China*
[2]*State Key Laboratory of Quantum Optics Technologies and Devices, Institute of Opto-Electronics, Taiyuan* 030006*, China*
[3]*Collaborative Innovation Center of Extreme Optics, Shanxi University, Taiyuan* 030006*, China*

Appendix A Asymmetric fractional OAM superpositions

In the fractional OAM mode, the phase jump is not an integer multiple of 2π, and the interval between adjacent topological charges is non-integer. The plane wave ψ_1 of the fractional OAM superpositions can be decomposed into the basis of integer OAM modes [1]

$$\psi_1(\rho,\theta,z)=\sum_{m'=m_{\min}}^{m_{\max}} c_{m'}\mu_p^{m'}(\rho,\theta,z). \tag{A1}$$

Here $m_{\min}=\mathrm{Rnd}[M-n_{modes}/2]$, $m_{\max}=m_{\min}+n_{modes}-1$, $M=m+\mu$ represents the fractional topological charge, where m and $\mu\in(0,1)$ are the integer and fractional parts of the topological charge respectively, and n_{modes} denotes the finite number of contributing modes in the superposition. The integer OAM modes $\mu_p^{m'}(\rho,\theta,z)$ can be described by the Laguerre-Gaussian functions in cylindric coordinates [1], and the coefficient $c_{m'}$ is given by

$$c_{m'}=\exp(-i\mu\alpha)\frac{i\exp[i(M-m')\theta_0]}{2\pi(M-m')}\quad[\exp[i(M-m')\alpha](1-\exp(i\mu 2\pi))]. \tag{A2}$$

Here, we set the radial index as $p=0$, α is the orientation of the edge dislocation within the range of 0 to 2π [2,3], and the angle θ_0 is an arbitrary starting point for the azimuthal angle.

Besides the plane wave of the fractional OAM superpositions, there is also the spherical wave of the fractional OAM superpositions. The spherical wave ψ_2 can be expressed in cylindrical coordinates [4]

$$\psi_2(\rho,\theta,z)=(\frac{\rho\sqrt{2}}{w(z)})^{|M|}\exp(-\frac{\rho^2}{w^2(z)})\exp(\mathrm{i}M\,\theta)\frac{1}{z}\exp(-ikz(1+\frac{\rho^2}{2z^2})). \tag{A3}$$

The Gaussian spot size is represented by the parameter $w(z)$, which is given by

$$w(z)=w_0\sqrt{1+(\frac{z}{z_R})^2}, \tag{A4}$$

where z_R denotes the Rayleigh range, and w_0 indicates the waist radius.

Here, we consider the superposition of the plane wave and spherical wave, which can be applied to generate the asymmetric fractional OAM superpositions ($|\psi\rangle=|\psi_1\rangle+\exp(i\phi)|\psi_2\rangle$). In the asymmetric fractional OAM superpositions, the plane wave $|\psi_1\rangle$ has a positive (negative) fractional topological charge and the spherical wave $|\psi_2\rangle$ has a negative (positive) fractional topological charge, and the absolute value of the two topological charges are different. The phase holograms of the asymmetric fractional OAM superpositions are shown in Fig. A1.

Appendix B Neural network architecture

For identifying the fractional topological charges of the OAM superposition states, we construct a neural network architecture. We use the images with a resolution of 224×224 pixels as input. Each module includes a 3×3 convolutional layer (Conv), a rectified linear unit (ReLu) and a 2×2 max-pooling layer. The image undergoes preliminary feature extraction through a Conv. Then the ReLu activation function is applied to introduce nonlinearity to enhance the expressive power

* Corresponding author (email: Suxl@sxu.edu.cn)

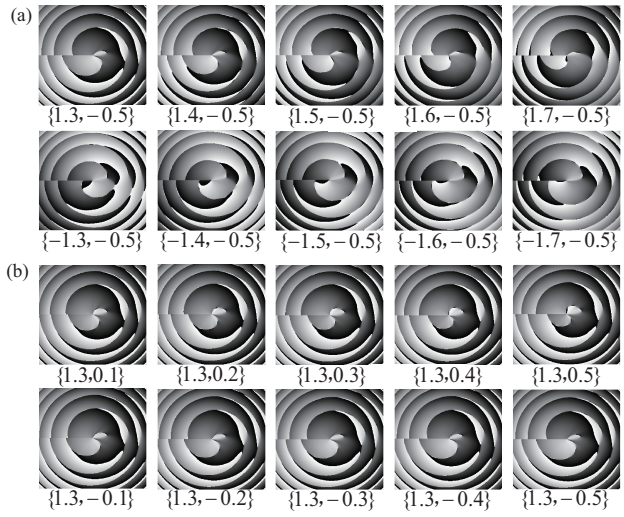

Figure A1 The phase images of the asymmetric fractional OAM superpositions. (a) The topological charge of the plane wave changes and the spherical wave at $l = -0.5$. (b) The topological charge of the spherical wave changes and the plane wave at $l = 1.3$.

of neural networks. After that, a max-pooling layer halves the feature map size, thereby selecting the most representative features. In the fourth pooling layer, average pooling is utilized instead of max-pooling to smooth the feature map. After four modules, the spatial size of the feature map is reduced to 14×14 pixels and then connected to the fully connected layer (FC). To reduce the risk of overfitting, a Dropout layer is added after the FC. At the output, a softmax layer is applied to perform multi-class classification, where the class with the highest predicted probability is selected as the final class. The network architecture occupies 101.15 MB of memory, which maintains high efficiency and achieves structural simplicity.

The experimental platform is built on the Windows operating system and features a robust hardware configuration. It includes an Intel Xeon Platinum 8255C processor with 12 virtual cores operating at a clock frequency of 2.25 GHz and an NVIDIA GeForce RTX 2080 Ti Graphics Processing Unit (GPU) supporting high-performance parallel computing. Additionally, RAM with 40 GB is equipped to ensure ample resources for complex data processing and multitasking. The neural network is trained in the PyTorch framework and the parameters are updated using the Adam optimizer with the learning rate set at 1×10^{-4}.

The accuracy of the model's predictions is quantified by the cross-entropy loss function, which is defined as follows

$$\text{Cross-Entropy Loss} = -\sum_{j=1}^{C} y_{i,j} \log(p_{i,j}). \tag{B1}$$

Here, C represents the total number of categories, $y_{i,j}$ denotes the true label of the i sample on j category, and $p_{i,j}$ is the predicted probability. By minimizing the cross-entropy loss, the model can optimize its parameters, thereby improving the accuracy of its predictions. The detailed parameters of the neural network are presented in Table B1.

Table B1 Parameters of Neural Network

Hyper-parameter	Value
Batch size	4
Epoch	50
Iteration	20520
Initial learning rate	0.0001

.

Appendix C Supplemental experimental results

After the training, the model parameters with the highest accuracy are saved for subsequent testing. The test results of 19-class classification tasks of the asymmetric fractional OAM superpositions are presented in Fig. C1, where the confusion matrix compares the model's predicted labels and the samples' true labels. The accuracy of the model on the test set is 99.34%.

When the larger topological charge is chosen, the accuracy will decrease if the number of datasets is not increased. With the increase of topological charge, the challenges mainly come from the larger aperture size and more complex intensity distribution of the OAM beams in the experimental datasets, which increases the identification difficulty of CNN [5, 6].

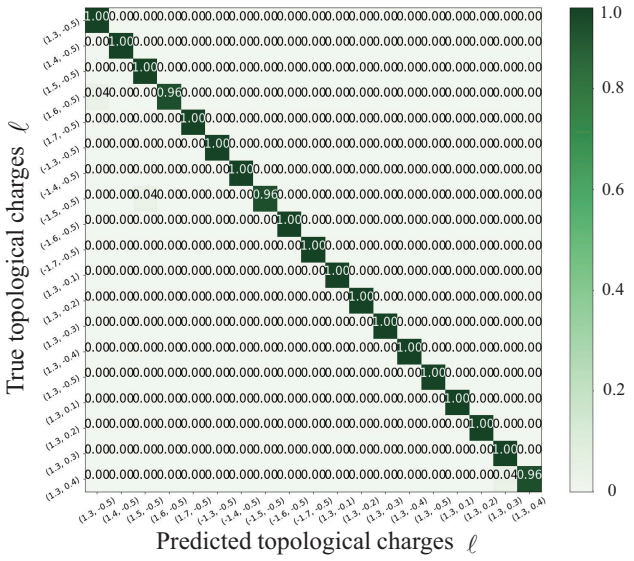

Figure C1 Confusion matrix of 19-class classification tasks of the asymmetric fractional OAM superpositions.

The challenge of the larger aperture size of the OAM beam with high-order topological charges may be solved by using the Laguerre-Gaussian mode coaxial superposition method [7]. This method uses a coaxial superposition of suitable low-order Laguerre-Gaussian modes as the initial optical vortex arrays, and devises a mathematical algorithm to multiply these vortices into arbitrarily high orders, while the array structure remains unchanged. The other challenge of the complex intensity distribution of the OAM beam with high-order topological charges may be solved by increasing the diversity of the experimental datasets and optimizing the CNN parameters.

References

1 J. B. Götte, K. O'Holleran, D. Preece, et al. Light beams with fractional orbital angular momentum and their vortex structure. Opt. Express, 2008, 16: 993-1006.
2 S. S. R. Oemrawsingh, A. Aiello, E. R. Eliel, et al. How to observe high-dimensional two-photon entanglement with only two detectors. Phys. Rev. Lett., 2004, 92: 217901.
3 A. Aiello A, S. S. R. Oemrawsingh, E. R. Eliel, et al. Nonlocality of high-dimensional two-photon orbital angular momentum states. Phys. Rev. A, 2005, 72: 052114.
4 X. Li, Y. Tai, F. Lv, et al. Measuring the fractional topological charge of LG beams by using interference intensity analysis. Opt. Commun., 2015, 334: 235-239.
5 W. Xiong, Y. Luo, J. Liu, et al. Convolutional neural network assisted optical orbital angular momentum identification of vortex beams. IEEE Access, 2020, 8: 193801.
6 H. Zhang, J. Zeng, X. Lu, et al. Review on fractional vortex beam. Nanophotonics, 2022, 11: 241-273.
7 W. Zhang and L. Chen. High-harmonic-generation-inspired preparation of optical vortex arrays with arbitrary-order topological charges. Chin. Opt. Lett., 2018, 16: 030501.